X-ray Crystal Structure of γ-Chymotrypsin in Hexane[†,‡]

Neela H. Yennawar, Hemant P. Yennawar, and Gregory K. Farber*

Departments of Chemistry and Biochemistry and Molecular Biology, and Center for Biomolecular Structure and Function, 152 Davey Laboratory, The Pennsylvania State University, University Park, Pennsylvania 16802

Received February 21, 1994; Revised Manuscript Received March 24, 1994[⊗]

ABSTRACT: Crystals of γ-chymotrypsin grown in aqueous solution were soaked in *n*-hexane, and the structures of both the soaked and the native crystals were determined to 2.2-Å resolution. Seven hexane molecules and 130 water molecules were found in the hexane-soaked crystals. Two of the seven hexane molecules are found near the active site, and the rest are close to hydrophobic regions on or near the surface of the enzyme. In the hexane structure, water molecules that were not observed in the native structure form a clathrate around one of the hexane molecules. Only 97 water molecules were found in the native structure. The temperature factors for atoms in the hexane environment are lower than those in the aqueous environment. There are significant changes between the two structures in the side chains of both polar and neutral residues, particularly in the vicinity of the hexane molecules. These changes have perturbed the hydrogen-bonding patterns. The electron density for the peptide bound in the active site has been dramatically altered in hexane and appears to be tetrahedral at the carbon that is covalently bound to Ser 195. The crystalline enzyme retains its active conformation in the nonpolar medium and can catalyze both hydrolysis and synthesis reactions in hexane.

In recent years there has been interest in the properties of chymotrypsin and other enzymes in nonaqueous solvents. A number of advantages have been reported for enzymes suspended in organic solvents. These include increased thermostability (Zaks & Klibanov, 1984), altered substrate specificity (Zaks & Klibanov, 1986, 1988a; Gololobov *et al.*, 1992; Tawaki & Klibanov, 1992), and the possibility of catalyzing reactions that are thermodynamically or kinetically impossible in water (Homandberg *et al.*, 1978; Zaks & Klibanov, 1985; Kuhl *et al.*, 1990; Stahl *et al.*, 1990; West *et al.*, 1990; Kasche *et al.*, 1991).

Chymotrypsin is an ideal model system to explore the effects of organic solvents on enzymatic catalysis. The chemical and kinetic mechanisms of chymotrypsin have been studied for decades (Polgar *et al.*, 1987), and a number of structural studies have been reported (Steitz & Shulman, 1982). The placement of chymotrypsin in organic solvents dramatically alters substrate specificity. Adlercreutz and co-workers have demonstrated that the specificity in the P1′ site changes when chymotrypsin is suspended in a solution of acetonitrile, dimethylformamide, and water (Gololobov *et al.*, 1992). Zaks and Klibanov (1986) have demonstrated that the specificity in the P1 site also changes when chymotrypsin is suspended in dry octane. Two groups have reported that chymotrypsin-catalyzed peptide bond synthesis is possible in organic solvents (Homandberg *et al.*, 1978; Kasche *et al.*, 1991). Some of these reports also show that chymotrypsin can use D-amino acids as substrates in organic solvents (Stahl *et al.*, 1990; West *et al.*, 1990).

Several models have been proposed to explain this altered reactivity. Zaks and Klibanov (1988a) propose that the increased thermostability in organic solvents is due to high kinetic barriers between the native and the unfolded states. Tawaki and Klibanov (1992) propose that changes in substrate specificity can be explained by altered substrate binding in organic solvents. Hartsough and Merz (1992, 1993) have begun to address the effect of nonaqueous solvents on protein structure using molecular dynamics simulations. They suggest that the inherent flexibility of proteins in nonaqueous media does not change. Rather, they propose that many of the weak intramolecular forces that stabilize proteins (hydrogen bonds, salt bridges) are stronger in organic solvents than in water. Their simulations predict that side-chain positions for amino acids on the surface of the protein should be significantly altered in organic solvents.

Clearly, a structural study of enzymes in organic solvents is necessary to answer the questions raised by these competing models and to explain the structural basis for altered enzyme reactivity in organic solvents. The structure of glutaraldehyde-cross-linked crystals of subtilisin in acetonitrile has recently been reported (Fitzpatrick *et al.*, 1993). We now report the refined crystal structures of γ-chymotrypsin in both aqueous (native structure) and hexane environments at 2.2-Å resolution. Unlike subtilisin in acetonitrile, crystals of γ-chymotrypsin in hexane do not require cross-linking for stability. This form of chymotrypsin was chosen because it already has a peptide bound in the active site (Dixon & Matthews, 1989; Harel *et al.*, 1991; Dixon *et al.*, 1991), so that it has a built-in probe for changes in substrate binding.

MATERIALS AND METHODS

α-Chymotrypsin (Sigma, C-4129) was converted to γ-chymotrypsin and was crystallized as described previously (Stoddard *et al.*, 1990), with one addition. After the final solution was dispensed into a 0.5 dram vial, a fiber that had been dipped into a solution containing γ-chymotrypsin crystals was briefly dipped into the new crystallization solution. This seeding technique greatly improved the likelihood of obtaining large single crystals (0.5 × 0.5 × 0.8 mm). Crystals typically appeared within 3 days and grew to full size in 10 days.

[†] This work was supported by the Office of Naval Research and the Searle Scholars Program.

[‡] The coordinates have been deposited in the Brookhaven Protein Data Bank under the file names 1GMD for the hexane structure and 1GMC for the native structure. Coordinates are also available by sending e-mail to FARBER@RETINA.CHEM.PSU.EDU.

* Author to whom correspondence should be addressed at the Department of Chemistry.

[⊗] Abstract published in *Advance ACS Abstracts,* May 15, 1994.

0006-2960/94/0433-7326$04.50/0

Table 1: Data Collection and Data Reduction Statistics

	native	hexane
space group	$P4_22_12$	$P4_22_12$
unit cell dimensions (Å)		
a	69.54	69.34
b	69.52	69.32
c	98.01	97.51
no. of reflections[a]		
collected	16994	13982
observed (>2σ)	8058	7606
resolution (Å)	2.2	2.2
no. of crystals	3	4
R_{merge} (%)[b]	6.4	9.2
isomorphous difference[c] (%)	15.3	

[a] The hexane data sets were collected using crystals completely surrounded by hexane. [b] $R_{merge} = \Sigma|I_j - \bar{I}|/\Sigma\bar{I}$, where j is a summation over all crystals. [c] Isomorphous difference = $\Sigma|F_{nat} - F_{hex}|/\Sigma F_{nat}$, where the summation is over all common reflections.

The crystals were then transferred to thin-walled quartz capillary tubes, and the hexane soaks of the crystal were done directly in the capillary tube. The size of the capillary tube was chosen so that the crystal would wedge roughly halfway down the tube. *All* of the aqueous solution was removed from the capillary tube using filter paper. Any water left in the capillary tube would form a drop centered at the crystal. The capillary tube was then flushed repeatedly with anhydrous *n*-hexane (HPLC grade from Aldrich) that had been stored over 4-Å, $^1/_8$-in., 4–8 mesh molecular sieves. The concentration of water in the hexane that was placed around the crystal was less than 10 nM, as determined using a Mettler DL-18 Karl-Fisher titrimeter. The capillary tube was sealed with sticky wax and allowed to sit for 24 h. Thereafter, the seal was broken and the hexane removed. A fresh volume of dry hexane was added to the capillary tube, along with pipe cleaner fibers to immobilize the crystal. The capillary was resealed and was mounted on a goniometer head for data collection. Crystals treated in this way rarely cracked. The native data set was collected on crystals mounted in capillary tubes with slugs of mother liquor at both ends. Very little liquid was left near the native crystals during data collection.

X-ray data were measured to a nominal resolution of 2.2 Å using a four-circle diffractometer with a rotating anode X-ray source (Molecular Structure Corporation). Table 1 lists the crystal data and data processing parameters. Radiation was monochromatized using a graphite crystal. Individual background measurements were made for all reflections. Data from different crystals were merged together using a set of 211 strong reflections, which were measured for each crystal (Monahan *et al.*, 1967). This common block of reflections was collected at the beginning and at the end of data collection. A radiation damage correction was applied as a function of both time and resolution using these reflections (Fletterick *et al.*, 1976). The crystals in hexane showed significantly reduced radiation damage as compared to those in water. The hexane data were scaled to the native data set using a single overall scale factor. Programs for data reduction were written in the authors' laboratory.

The starting point for the refinement of the two structures was the structure reported by Stoddard *et. al.* (1990) stripped of all of the water molecules and the cinnamate in the active site. Both the native and the hexane structures were refined independently using XPLOR (Brunger *et al.*, 1987). Results from the crystallographic refinement appear in Table 2.

Simulated annealing was done in three rounds, increasing the resolution at each round. In an individual macrocycle, the structure was heated to 3000 K and cooled in increments of 25 K. After each cooling step, 50 steps of molecular dynamics simulation were performed. The time step for each of these runs was 0.5 fs. Conventional positional and *B*-factor refinement followed the simulated annealing refinement. After the *R*-factor converged, difference Fourier maps ($F_{hexane} - F_{native}$) showed continuous electron density that could be attributed to hexane molecules. These hexane molecules were built into the map manually and tested for short contacts before they were incorporated into refinement. Parameters for the hexane molecules were extended from the methylene and methyl carbons of the protein, with the partial charge set to zero. Only those with reasonable temperature factors were retained. Seven hexane molecules refined successfully.

Table 2: Refinement Statistics

	native	hexane
no. of water molecules[a]	97	130
final *R*-factor (%)[b]	17.6	17.5
δ-bond (Å)[c]	0.011	0.012
δ-angle (deg)[c]	1.954	1.824
mean *B*-factor (Å^2)		
protein	5.4	4.4
water	19.3	17.1
hexanes	none	12.5[d]
active site peptide	16.6	21.1

[a] The number of heavy atoms in the native structure including the active site peptide is 1766. [b] The final *R*-factor was calculated using the 5–2.2-Å shell of data. [c] Root-mean-square discrepancies from ideal values. [d] For the 42 carbon atoms of the seven hexane molecules.

Analysis of the water structure was handled with great care. Electron density peaks often appeared in the ($2F_o - F_c$) maps as possible water molecules, but did not reappear after water had been added to the structure. Only waters that reappeared after further refinement were included in the final model. In the intermediate steps of the refinement, water molecules with temperature factors less than 25 Å^2 were kept in the model. In the final stages of refinement, the *B*-factor cutoff was relaxed to 50 Å^2 because of the persistent reappearance of some of the peaks. There was a total of 97 water molecules in the native structure and 130 in the hexane structure.

After the water structure was completed, $2F_o - F_c$ maps showed clear continuous electron density in the active site. As has been done by others, this electron density was initially modeled as a tetrapeptide with the sequence Pro-Gly-Ala-Tyr in both the native and hexane structures (Dixon & Matthews, 1989; Harel *et al.*, 1991; Dixon *et al.*, 1991). In both structures, there was density attached to the oxygen of Ser 195, so that the tetrapeptide was initially modeled as an acyl enzyme intermediate. Additional positional and *B*-factor refinement was performed after the tetrapeptide was added to the active site. In order to provide an unbiased structural model of the active site region, simulated annealing omit maps (Hodel *et al.*, 1992) for both structures were calculated using XPLOR. An 8-Å sphere centered at Ser 195 was defined as the omitted region. Atoms in the shell 8–11 Å from the serine were harmonically restrained to prevent them from moving into the omitted region. Simulated annealing was carried out beginning at an initial temperature of 1000 K, with cooling in increments of 25 K to a final temperature of 300 K. Surprisingly, the resulting omit maps strongly suggested that the carbon of the peptide attached to Ser 195 was tetrahedral in the hexane structure and planar in the water structure. After the tetrahedral intermediate was built in the hexane model, the refinement was concluded with positional and *B*-factor refinement. All molecular modeling was performed using the program O (Jones *et al.*, 1991).

Table 3: Buried Surface Area for the Hexane Molecules (in Å^2)[a]

hexane	surface area	SA in protein	SA with water	buried SA	SA exposed to water
401	333.79	86.35	56.86	247.44 (74%)	29.49
402	340.89	0	0	340.89 (100%)	0
403	335.94	139.12	137.29	196.82 (59%)	1.83
404	334.17	160.16	134.42	174.01 (52%)	25.74
405	328.46	0	0	328.46 (100%)	0
406	336.10	109.74	100.22	226.36 (67%)	9.52
407	331.72	151.38	37.70	180.34 (54%)	113.68

[a] The surface area for each hexane was calculated in the absence of the rest of the protein structure. The SA in protein calculation included only the protein atoms. The SA with water calculation included both protein and solvent atoms. The buried surface area is the surface area of the hexane in the absence of protein minus the surface area in the presence of only protein atoms. The surface area exposed to water is the difference between columns 2 and 3.

Surface areas for the hexane molecules were calculated using XPLOR. A water molecule with a radius of 1.6 Å was used as the surface area probe. The surface area of each hexane was calculated with no protein present (surface area), with protein atoms present (SA in protein), and with protein and water molecules present (SA with water). All of these surface areas are reported in Table 3.

Crystals of chymotrypsin were shown to be active for the hydrolysis reaction in hexane using *p*-nitrophenyl acetate as a substrate (Hartley & Kilby, 1954). A large crystal (0.7 × 0.7 × 0.5 mm) of γ-chymotrypsin in hexane was mounted in a flow cell (Petsko, 1985). As described above, the crystal was placed in a capillary tube, water was removed from the tube, and hexane was added. Crystals were allowed to soak in hexane for at least 3 days before the experiment began. To construct the flow cell, polyethylene tubing with a small inner diameter (Intramedic, PE-190) was attached to both ends of the capillary tube. *p*-Nitrophenyl acetate (Aldrich N1990-7) was dissolved in acetonitrile to a concentration of 30 mM. A reservoir containing a solution of 99% hexane and 1% acetonitrile (containing an overall concentration of 0.3 mM *p*-nitrophenyl acetate) was attached to one of the tubes. The other tube was attached to a quartz flow cell mounted in a Hewlett-Packard HP 8452 diode array spectrophotometer. The flow rate was roughly 0.3 mL/min. The production of nitrophenol was monitored at 400 nm. The results of a typical experimental run are shown in Figure 1.

RESULTS

Enzyme Activity in the Crystal. Figure 1 shows that the crystals are catalytically active in the hydrolysis direction. The number of active sites in the crystal can be calculated from the size and the known density of the crystal. The equilibrium absorbance reading is what would be expected if every molecule in the crystal were catalytically active. The biphasic nature of the rise in absorbance could be due to either the slow diffusion through the crystal or the known burst kinetics of this substrate (Hartley & Kilby, 1954).

Comparison of the Hexane and Native Structures. The backbone conformation of the protein shows no major differences between the two structures (Figure 2). The RMS deviation for the backbone atoms is 0.17 Å. However, some of the side chains do show significant rearrangements, particularly those in the neighborhood of the hexane molecules. The RMS deviation for all non-hydrogen atoms between the two structures is 0.85 Å.

There are two types of sites in which the hexanes are localized: one where they replace water molecules and the other where they are adjacent to hydrophobic patches of the protein. In the former type, the hexane molecules disrupt the hydrogen-bonding pattern seen in the native structure and cause the side chains to reorient. Hexanes 401, 402, and 405 replace water molecules. Hexane 401 replaces waters 253 and 294 in the native structure, hexane 402 replaces water 297 (Figure 3), and hexane 405 replaces water 258. Hexanes 403, 404, and 406 bind in sites that had no water in the native structure. Hexane 407 binds close to an existing water site (309) and causes a cage of 12 water molecules to bind around the hexane site. Most of the waters forming this clathrate were not observed in the native structure.

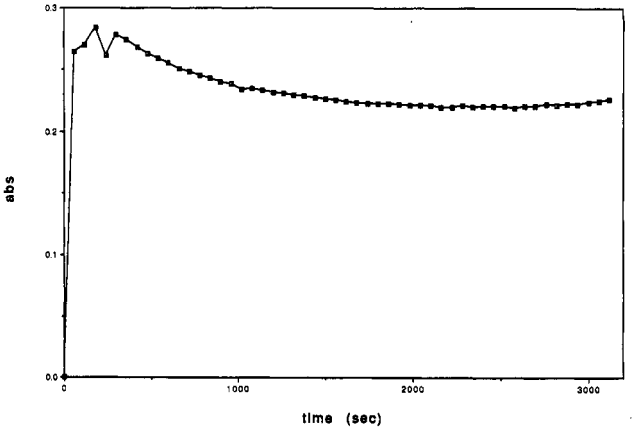

FIGURE 1: Burst and steady-state phases in the hydrolysis of *p*-nitrophenyl acetate by chymotrypsin crystals soaked in hexane.

Examples of hexane binding are shown in Figures 3 and 4. In Figure 3, hexane 402 binds in a relatively hydrophobic environment and replaces water 297. In addition to displacing a water, the binding of hexane 402 causes the side chain of Val 137 to rotate around the bond between the α- and β-carbons. The binding of hexane 407 (Figure 4) causes the side chain of Thr 37 to rotate, such that the terminal methyl group now shows a favorable van der Waals interaction with hexane (407, C1). The hydroxyl group of Thr 37 forms a new hydrogen-bond interaction with the terminal oxygen of the Asp 35 side chain. Ser 92 (in the $-x, -y, z$ symmetry-related molecule), which was hydrogen bonding with the hydroxyl group of Thr 37 in the native structure, reorients and now forms a hydrogen bond with a new water molecule (271) in the hexane structure.

As predicted by a molecular dynamics study of BPTI (Hartsough & Merz, 1993), charged residues seem to cluster closer in the hexane structure as compared to the native structure. Figure 5 shows one such example where the Asn 48, Glu 49, and Asn 50 side chains come closer to each other, increasing their electrostatic interactions. Another example of this clustering is shown in Figure 6, where the binding of hexane 403 (6.8 Å away) causes the side chain of Lys 177 to rotate by roughly 180°. In the hexane structure, the NZ (Lys 177) atom forms a new hydrogen bond with OG1 (Thr 98). The OG1 of Thr 98 also forms a hydrogen bond with Asn 95, which in turn forms a hydrogen bond with water 274. None of these hydrogen-bond interactions are observed in the native structure.

Long-Range Effects of Hexane. In the hexane structure, the organic molecules not only have caused changes in residues close to the binding sites but they have also had effects on the structure far away from the binding sites. Many examples of the strengthening of electrostatic and hydrogen-bond

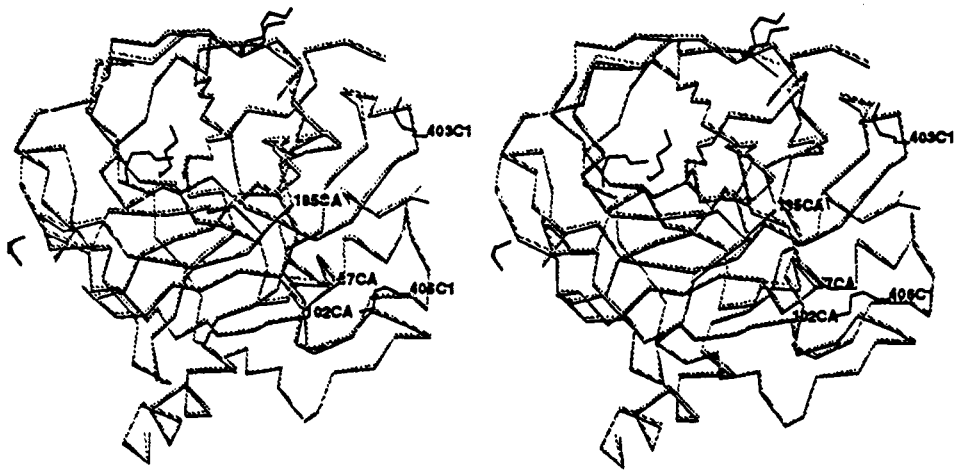

FIGURE 2: Stereoview of the superposition of the α-carbon trace of chymotrypsin in the hexane (dark) and native (light) structures. The catalytic triad, Ser 195, His 57, and Asp 102, is marked. The seven hexane molecules are plotted as thick lines. Two of them are in the proximity of the active site.

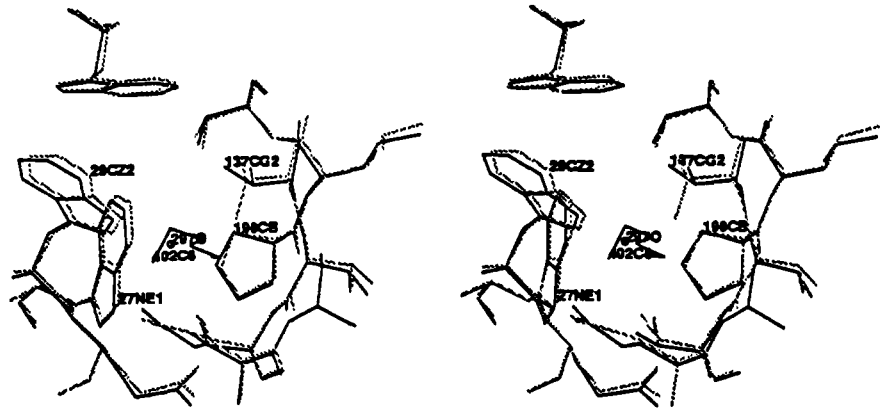

FIGURE 3: Hexane 402 occupies a totally hydrophobic pocket lined by Trp 27, Trp 207, and Val 137. The hexane replaces a water molecule (297 O1) of the native structure.

interactions can be seen. Three of the most dramatic cases are discussed below.

Two surface lysine side chains, Lys 36 and Lys 202 (from the $0.5 + x, 0.5 - y, 0.5 - z$ symmetry-related molecule), were pointing into the solvent channel in the native structure. These lysines rotate by more than 90° to face each other in the hexane structure (Figure 7). A water molecule (344) and a carbonyl oxygen (Gly 205) bridge the two lysine side chains by accepting hydrogen bonds from the NZ atoms.

A second example (Figure 8) can be seen at Gln 239. In the hexane structure, the NE2 atom of Gln 239 forms hydrogen bonds with two water molecules (285 and 343) that were not present in the native structure. Water 285 is also within hydrogen-bonding distance of the carbonyl oxygen for residue 124. The OE1 of Gln 239 accepts a proton from the backbone amide of Ser 76 and donates a proton to the carbonyl oxygen of Gln 74 (from the $0.5 + x, 0.5 - y, 0.5 - z$ symmetry-related molecule). None of these interactions (with the possible exception of the hydrogen bond between 239 OE1 and 76N) are observed in the native structure.

An excellent example of the burial of a hydroxyl group in the protein in hexane can be seen at Thr 110. In water, both the methyl and the hydroxyl groups of the Thr 110 side chain are exposed to the solvent (Figure 9). In hexane, the side chain rotated to bury the hydroxyl group and expose only the methyl group. Interestingly, a neighboring lysine residue (84) shows little rearrangement.

Hydrogen Bonds. There are 211 intraprotein hydrogen bonds common to both the native and hexane structures. Prospective hydrogen bonds were accepted if they had a donor to acceptor distance of less than 3.3 Å and a donor to acceptor to hydrogen angle of 90° or less. The hydrogen positions from XPLOR were used to determine this angle. There are 28 unique hydrogen bonds in the hexane structure and 19 in the native structure. These unique hydrogen bonds are listed in Tables 4 and 5. The 211 common hydrogen bonds are listed in the supplementary material.

The differences in hydrogen bonds between the native and hexane structures arise because of side-chain reorientations in the hexane environment and because of the larger number of water molecules in the hexane structure. There are 142 probable hydrogen bonds between the protein and water molecules in the native structure compared to 150 in the hexane structure. As expected from the greater number of water molecules in the hexane structure, the total number of hydrogen bonds between water molecules has increased from 15 in the native structure to 27 in the hexane structure.

There is a dramatic increase in the number of intermolecular hydrogen bonds between symmetry-related molecules in the crystal lattice from 26 in the native structure to 52 in the hexane structure. The increase in the overall number of hydrogen bonds in the hexane structure is consistent with the slight shrinkage of the lattice itself (Table 1). This agrees very well with the molecular dynamics simulation results for BPTI, where there was a profound increase in the hydrogen-bond network in a chloroform environment (Hartsough & Merz, 1993).

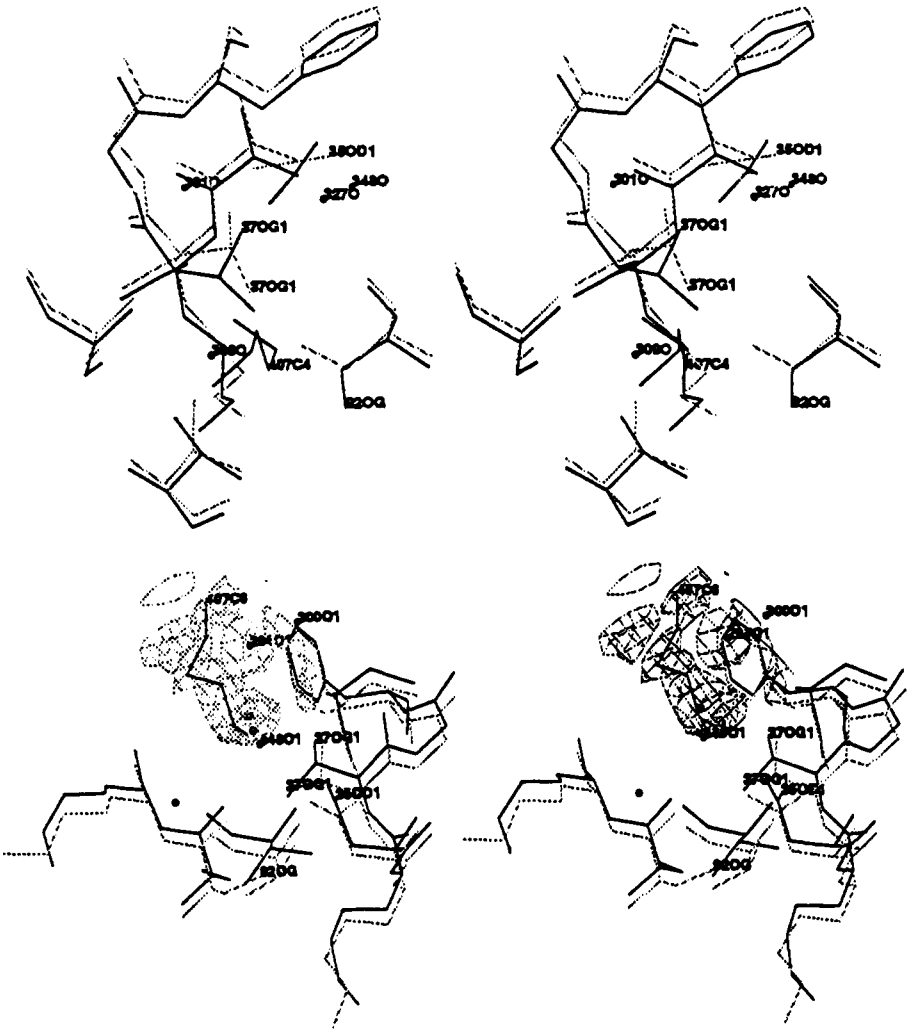

FIGURE 4: (A, top) Hexane 407 causes considerable rearrangement of the Thr 37, Asp 35, and Ser 92 side chains. It replaces a water molecule (309 O1) of the native structure (light) and has a favorable van der Waals interaction with 37 CG2. The 35 OD1 accepts two new hydrogen bonds in the hexane structure (dark): one from 37 OG1 and the other from a water molecule (448 O1). The 92 OG, which was hydrogen bonding with OG1 of Thr 37 in the native structure, now participates in a new hydrogen bond with water 271. The water clathrate around hexane 407 is not shown in this figure. B (bottom) shows the electron density from the original map, which was used to build the hexane positions.

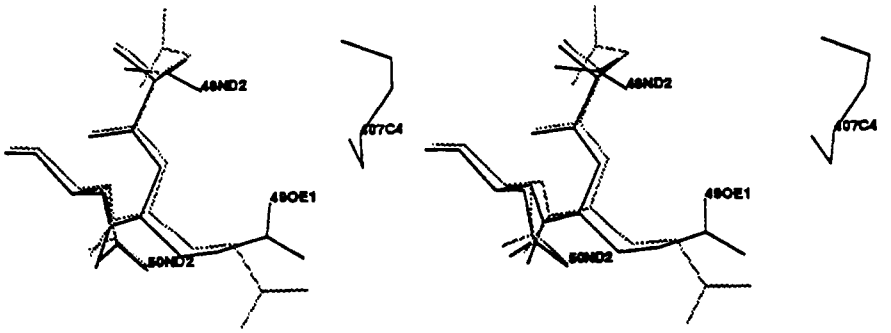

FIGURE 5: Hexane 407 causes the polar residues Asn 48, Glu 49, and Asn 50 to cluster closer to each other. The distance between 48 CG and 50 OD1 decreases from 7.9 Å in the native structure (light) to 6.4 Å in the hexane structure (dark). The distance between 50 OD1 and 49 CD decreases from 7.1 to 5.6 Å.

Active Site. Of the seven hexanes, two are within a 7-Å radius of the active site. One of these hexane molecules (406) is close to His 57 (one of the residues of the catalytic triad), and the other (403) is just outside the specificity pocket. The electron density map for the active site of the hexane structure is shown in Figure 10. It is clear from this map that the geometry around the carbon attached to the γ-oxygen of Ser 195 is tetrahedral, not planar as would be expected for the acyl enzyme intermediate. Our interpretation of the active site (including the hydrogen-bonding pattern) is shown in Figure 11.

There is clear continuous density for all four bonds to the tetrahedral carbon in the hexane structure. The density is significantly different from that observed in the native structure. The native structure shows a covalent acyl enzyme intermediate similar to those reported previously (Dixon & Matthews, 1989; Harel *et al.*, 1991; Dixon *et al.*, 1991). The peptide attached to Ser 195 in the native structure has been

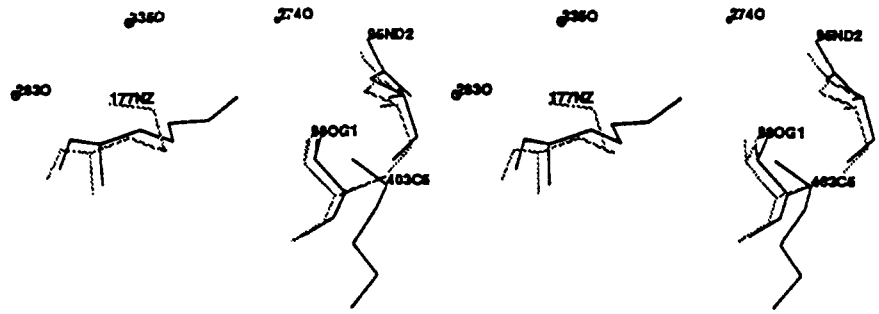

FIGURE 6: Hexane 403 causes the side chain of Lys 177 to rotate and form a hydrogen bond between 177 NZ and the OG1 of Thr 98. In the native structure (light), the sidechain was extended toward the solvent.

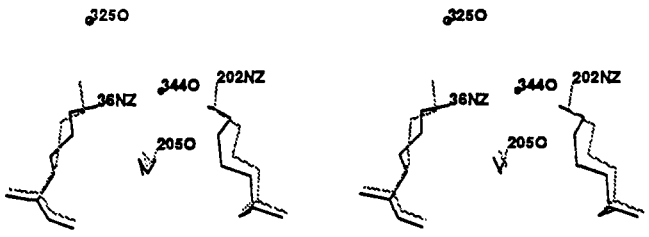

FIGURE 7: In the hexane structure (dark), two surface lysine residues, 36 and 202, rotate toward each other and form a closed loop interaction with water 344 and the Gly 205 backbone carbonyl oxygen. In the native structure, the lysine side chains are pointing outward into the solvent channel.

modeled as having the sequence Pro-Gly-Ala-Tyr, presumably coming from a Pro-Gly-Val-Tyr-Ala-Arg sequence in chymotrypsin. The tyrosine of this peptide is bound in the specificity pocket.

In the hexane structure, the density for the peptide continues in both directions from the tetrahedral carbon. The new density can be interpreted as either Asp or Asn, and we have modeled it as an Asp on the basis of the hydrogen-bonding pattern. No density is seen for any additional amino acids beyond the Asp. Since neither Asp nor Asn follows Tyr in the chymotrypsin sequence, we believe that we have trapped an intermediate in the synthetic direction. The peptide containing the attacking Asp presumably is produced when α-chymotrypsin is converted into γ-chymotrypsin. It has been shown that this process produces a large number of different peptides, which bind in the crystal (Harel *et al.*, 1991). The oxygen bound to the tetrahedral carbon forms two strong hydrogen bonds to the peptide backbone (residues 193 and 195). The oxygen is situated precisely in the oxy anion hole, 2.89 Å from the backbone amide of residue 193 and 2.92 Å from the backbone amide of residue 195. This oxygen has a third interaction with the δ-oxygen of the attacking aspartic acid.

In addition to changes at the P1 and P1′ positions of the peptide, there are some differences in the way the peptide binds in the rest of the active site in hexane. At the P2 site (modeled as an Ala), the peptides in the native and the hexane structures are very similar. However, the model is quite different in the P3 and P4 sites (Gly-Pro). In both the native and the hexane structure, we see density for two different peptide sites in these positions. Since the peptide is heterogeneous (Harel *et al.*, 1991), it is possible that the density should be interpreted as two peptides each with partial occupancy. Alternatively, it is possible that the Tyr-Ala/Val-Gly-Pro peptide has two possible binding conformations. The branch of electron density that predominates in the water structure is not the same as the branch that dominates the hexane structure. Since the peptide must bind in the crystallization solution, and since the crystals that were used to collect the native data set were grown in the same manner as those that were used for the hexane structure, it seems likely that the peptide has two different conformations. Hexane alters the relative occupancies of these two conformations.

B-Factor Comparison. A differential temperature factor plot ($B_{native} - B_{hexane}$) is shown in Figure 12. Positive peaks in this figure correspond to amino acids that have a higher *B*-factor in the native structure than in hexane. The figure clearly shows that there are many more positive peaks than negative peaks. The negative peaks correspond to hydrophobic or neutral stretches on the surface of the enzyme. In addition to the protein atoms, the water molecules in the hexane structure also have lower *B*-factors. This is indicated by their mean temperature factors (19.3 Å^2 for the 97 water molecules in the native structure and 17.1 Å^2 for the 130 water molecules in the hexane structure).

DISCUSSION

Protein Structure. The goal of this study was to begin to develop a structural basis for the altered properties that are observed when an enzyme is suspended in an organic solvent. The easiest property to explain is the increased thermostability of proteins in organic solvents. Klibanov and co-workers have argued that proteins are more rigid in organic solvents (Zaks & Klibanov, 1988a). They further argue that this rigidity is responsible for the increased thermostability (Zaks & Klibanov, 1984, 1988a). Our structures support these arguments. The thermal factors in a protein crystal are one measure of protein flexibility. Thermal factors can be high due to either static disorder in the crystal lattice or motion that occurs during the diffraction measurement. Comparison of thermal factors can be especially difficult when a data set is measured from more than one crystal since the thermal factors may be different (due to different handling, for example), even for crystals from the same batch. Table 2 and Figure 12 show that the thermal factors for both protein atoms and for water molecules in the hexane structure are significantly lower than those for the native structure. Because of the problems in comparing thermal factors, this observation supports the idea that the enzyme is more rigid, but it is not conclusive proof.

Strong supporting evidence for decreased mobility comes from the diffraction limits of the crystals in hexane compared to those in aqueous solution. During data collection for the native data set, the crystals were surrounded mainly by air. In contrast, the crystals for the hexane data set were surrounded by hexane, which absorbs X-rays much more than air. Despite this increased absorption, the crystals in hexane had the same number of observed reflections in the outermost shells as the native structure. The only reasonable explanation for this is that the hexane crystals intrinsically diffract more strongly than the native crystals. Diffraction limits increase as the

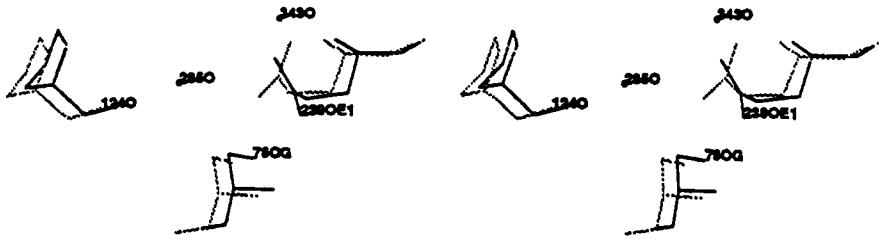

FIGURE 8: Gln 239 participates in a new hydrogen-bond network in the hexane structure. The NE2 atom hydrogen bonds with two water molecules 343 and 285. Gln 239 OE1 accepts a proton from the backbone amide of Ser 76. Water molecule 285 donates a proton to the Pro 124 carbonyl oxygen.

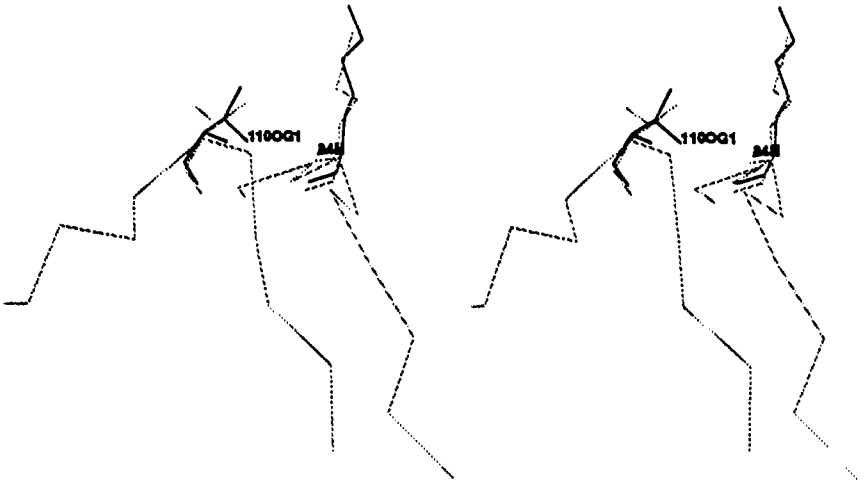

FIGURE 9: C-α trace from Ser 109 to Ser 113 and from Lys 82 to Lys 85 in the native structure is shown as a light line. The OG1 of Thr 110, which was solvent-exposed in the native structure, rotates toward the protein and accepts a hydrogen bond from the backbone amide of Lys 84.

order in a crystal lattice increases, and the order in the lattice of a protein crystal increases as the protein becomes more rigid. This increased rigidity is seen for both of the protein atoms and for the water molecules near the surface of the protein. Comparison of $2F_o - F_c$ maps for the native and hexane structures shows that the water peaks are stronger in the hexane structure. In addition, we see many more water molecules in the hexane structure compared to the native structure.

The molecular basis for this increased rigidity is probably the stronger interactions between polar groups in the hexane structure. Molecular dynamics simulations show that organic solvents should cause substantial side-chain rearrangements (Hartsough & Merz, 1992, 1993). These simulations suggested that hydrophobic groups would be more likely to be exposed in a nonpolar solvent and that hydrogen bonds and salt bridges would be stronger in nonpolar solvents than in water. Our structures provide many examples of these rearrangements.

In addition to being responsible for the increased thermostability, the side-chain rearrangements in the hexane structure explain the altered reactivity of enzymes in organic solvents. The differences that we observe between the native and hexane structures are on the same order of magnitude as those introduced by site-directed mutagenesis. It has been observed previously that mutagenesis can be used to change the rate of the principal reaction sufficiently that side reactions can become significant (Pompliano *et al.*, 1990; Wilks *et al.*, 1988). Our structures suggest that the altered substrate specificity seen in organic solvents is due to a similar phenomenon.

The large side-chain changes that we observe in hexane were not observed in the structure of subtilisin in acetonitrile (Fitzpatrick *et al.*, 1993). It is not clear whether the relatively small changes between the subtilisin structures are due to the different properties of acetonitrile compared to hexane or due to the fact that the subtilisin crystals in acetonitrile required glutaraldehyde cross-linking for stability.

Solvent Structure. We observe 33 more waters in the hexane structure than in the native structure. There are two causes for the significant increase in water molecules. One reason is the strong tendency of water to partition into the protein environment rather than the hexane environment. This observation confirms earlier suggestions that proteins in organic solvents retain at least a monolayer of water (Zaks & Klibanov, 1988b). The second reason is the formation of a water clathrate around one of the hexane positions (407).

We were initially surprised that three of the hexane molecules (401, 402, and 405) each displaced one or two water molecules. A surface area calculation suggests an explanation for this effect. The surface areas of the hexane molecules are given in Table 3. The buried surface area for the hexane molecules ranges from 174.01 to 340.89 Å^2. A reasonable estimate of the free energy for the transfer of a hexane molecule out of water to a nonpolar patch on the protein surface is –7.9 cal/mol/Å^2 (Ooi & Oobataka, 1988). Therefore, the free energy of binding for the hexane molecules in chymotrypsin varies from –1.4 to –2.7 kcal/mol. This free energy is on the same order of magnitude as the hydrogen bonds with one to two water molecules that were lost upon hexane binding.

Active Site. Crystal structures that have been interpreted as tetrahedral intermediates have been seen in a number of serine proteases, with various slow substrates or inhibitors (Sweet *et al.*, 1974; Bone *et al.*, 1987, 1989; Delbaere & Brayer, 1985; Rühlmann *et al.*, 1973; James *et al.*, 1980; Matthews *et al.*, 1975;, Tulinsky & Blevins, 1987; Marquart *et al.*, 1983). As in these earlier structures, the peptide backbones of residues

Table 4: Unique Protein–Protein Hydrogen Bonds in Hexane Structure[a]

	donor (D)	acceptor (A)	distance (Å)	angle (D–A–H) (deg)
1	37 N-H	37 OG1-CB	3.158	87.254
2	49 N-H	49 OE1-CD	3.167	38.977
3	51 N-H	48 OD1-CG	2.836	71.935
4	59 N-H	57 O-C	2.908	89.801
5	61 OG1-HG1	61 O-C	3.241	66.680
6	76 N-H	75 OG-CB	3.144	89.670
7	92 N-H	92 OG-CB	2.957	85.685
8	93 NZ-HZ1	91 OD1-CG	2.977	73.420
9	97 N-H	95 O-C	3.183	89.535
10	110 N-H	110 OG1-CB	2.887	81.285
11	110 OG1-HG1	110 O-C	2.827	51.967
12	116 N-H	115 OG-CB	2.818	86.490
13	134 OG1-HG1	131 O-C	2.893	53.024
14	164 OG-HG	164 O-C	3.183	68.525
15	166 N-H	166 OG1-CB	2.951	86.762
16	189 OG-HG	190 O-C	2.822	35.044
17	193 N-H	505 OD1-CG	3.067	47.553
18	217 N-H	504 OH-CZ	3.164	83.657
19	217 OG-HG	221 OG-CB	3.023	26.341
20	219 N-H	219 OG1-CB	3.005	86.210
21	219 OG1-HG1	219 O-C	3.058	57.688
22	221 N-H	221 OG-CB	2.851	81.065
23	221 OG-HG	221 O-C	3.198	57.966
24	221 OG-HG	224 OG1-CB	3.210	65.249
25	223 N-H	223 OG-CB	2.899	87.688
26	224 OG1-HG1	221 OG-C	3.210	78.651
27	241 OG1-HG1	237 O-C	3.042	20.842
28	502 N-H	216 O-C	2.789	73.530

[a] A distance cutoff of 3.2 Å between the donor and the acceptor and an angle cutoff of 90° at the acceptor was applied. Three of the hydrogen bonds discussed in the text and in the diagrams have not been included in the list because of these cutoffs. They are as follows: 37 OG1...35 OD1, 2.722, 91.438; 177 NZ...98 OG1, 3.357, 71.321; 202 NZ...205 O-C, 3.590, 27.009.

Table 5: Unique Protein–Protein Hydrogen Bonds in the Native Structure

	donor (D)	acceptor (A)	distance (Å)	angle (D–A–H) (deg)
1	26 OG-HG	23 O-C	2.733	25.477
2	48 ND2-HD21	48 O-C	3.234	59.230
3	58 N-H	56 O-C	3.116	78.625
4	61 N-H	61 OG1-CB	2.922	88.907
5	61 OG1-HG1	64 OD1-CG	3.006	38.510
6	63 N-H	63 OG-CB	2.962	86.822
7	74 N-H	72 O-C	3.163	86.360
8	75 OG-HG	77 OG-CB	3.049	85.477
9	97 N-H	96 OG-CB	3.217	89.908
10	125 N-H	125 OG-CB	2.834	81.821
11	139 OG1-HG1	30 OE1-CD	2.772	30.043
12	170 N-H	168 O-C	3.091	88.356
13	186 OG-HG	186 O-C	3.207	66.097
14	190 OG-HG	228 OH-CB	3.052	64.239
15	223 N-H	221 OG-CB	3.226	31.297
16	224 N-H	224 OG1-CB	2.893	88.805
17	224 OG1-HG1	224 O-C	3.152	59.642
18	229 N-H	214 OG-CB	3.087	72.076
19	244 N-H	242 O-C	3.225	85.401

in the P2–P4 sites in our hexane structure make the expected hydrogen bonds to the protein. The only significant difference is the interaction of the side chain of the attacking aspartic acid with the protein. In earlier structures, the residue in the P1′ position was either absent or did not make any strong interactions with the protein. This is understandable since this product usually dissociates in water once the scissile bond has been cleaved. In protein crystals in hexane, the equilibrium has apparently shifted to make binding at the P1′ site favorable. Such a shift in equilibrium toward peptide bond synthesis has been reported in other nonaqueous solvents (Homandberg *et al.*, 1978; Kasche *et al.*, 1991). The Asp side chain has three possible hydrogen-bonding interactions with the protein and one interaction with the hydroxyl attached to the tetrahedral carbon. This side chain is located where a highly conserved water molecule (the Henderson water) is usually observed in structures formed in water (Henderson, 1970; Singer *et al.*, 1993a,b; Perona *et al.*, 1993). We observe good density for the Henderson water in the native structure.

The Henderson water has been proposed as the water molecule that catalyzes the hydrolysis reaction (Perona *et al.*, 1993). This proposal is not supported by time-dependent structures obtained using the Laue method (Singer *et al.*, 1993a,b). The Laue structure has been interpreted as showing that the Henderson water is involved in the stabilization of the active site rather than in catalysis (Singer *et al.*, 1993b). Our structure in hexane supports the interpretation of the Laue structure. The amine of the attacking Asp group clearly comes from the direction of the water molecule that was observed in the Laue structures (water 1082). The side chain of the attacking Asp has displaced the Henderson water.

The proposal that any crystal structure has trapped the tetrahedral intermediate seems unlikely on energetic grounds. It has been estimated that the transition state that occurs between the ES complex and the acyl enzyme is 12 kcal/mol higher in free energy than the acyl enzyme intermediate (West *et al.*, 1990) under typical steady-state conditions. Therefore, 12 kcal/mol is a conservative estimate for the free energy difference between the tetrahedral intermediate and the acyl enzyme intermediate in the hexane-treated crystals. Since a crystal structure is an average over both crystal volume and time, the tetrahedral intermediate must be more stable than either the acyl enzyme intermediate or the ES complex. Knowles has shown that such stabilization of enzyme-bound intermediates can be achieved for proline racemase by very high substrate concentrations (Albery & Knowles, 1986). It is possible (but seems unlikely) that this is the cause of the stabilization of the tetrahedral intermediate in hexane.

While searching for an explanation of this problem, we noticed that Asp 102 makes two very short hydrogen bonds in the hexane structure. The 2.63-Å interaction is among the shortest hydrogen bonds in the entire structure. One possible explanation for the stability of the tetrahedral intermediates is these short hydrogen bonds. Short, strong hydrogen bonds have been implicated in a number of enzymatic reactions (Cleland, 1992; Gerlt *et al.*, 1991; Gerlt & Gassman, 1992, 1993). Unfortunately, this bond is also very short in a number of other serine protease structures that have no substrate in the active site (Tsukada & Blow, 1985).

A further argument against the thermodynamic trapping of tetrahedral intermediates in serine proteases is a series of NMR experiments that has clearly shown that tetrahedral intermediates are not directly observable between complexes of trypsin and the bovine trypsin inhibitor or the soybean trypsin inhibitor in solution (Baillargeon *et al.*, 1980; Richarz;*et al.*, 1980). Crystal structures of these complexes have been interpreted as forming a tetrahedral intermediate (Sweet *et al.*, 1974; Rühlmann *et al.*, 1973). It has been suggested that the difference between the crystal structures and the NMR structures is that water molecules are excluded from the active site in the crystal structures but not in the NMR experiments (Steitz & Shulman, 1982). If this explanation is correct, the tetrahedral intermediates observed crystallographically are kinetically trapped, rather than being thermodynamically more stable than the neighboring intermediates on the reaction pathway.

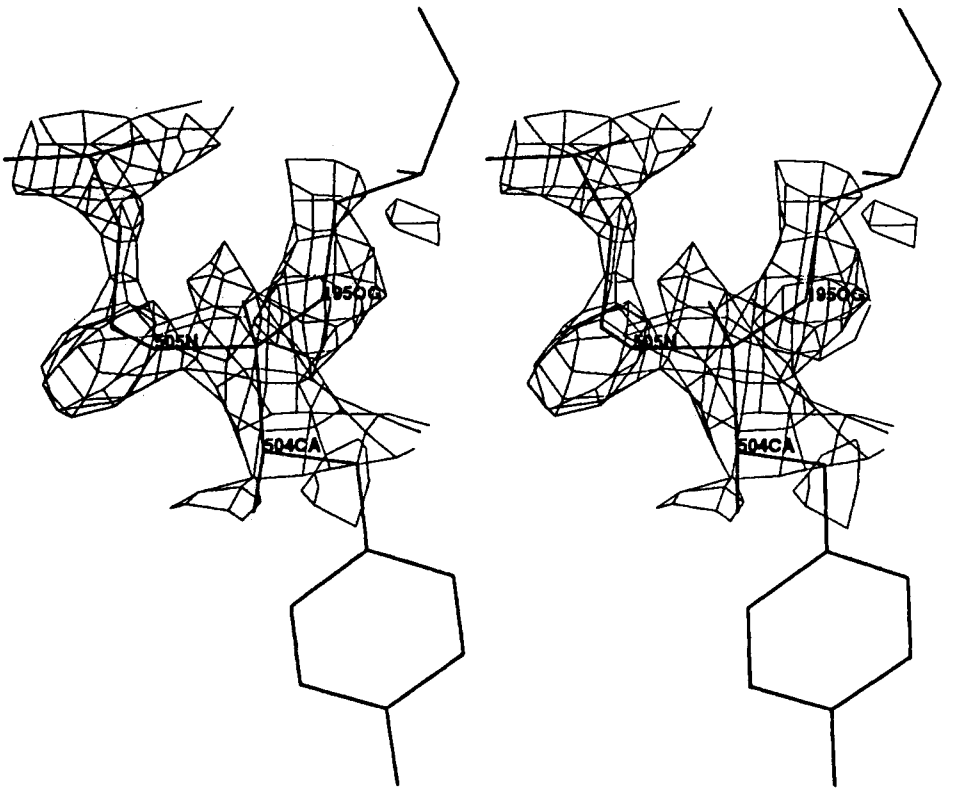

FIGURE 10: Residues of the catalytic triad and the peptide in the active site. The density attached to Ser 195 is clearly tetrahedral. The group attacking from the P1′ direction has been modeled as an Asp.

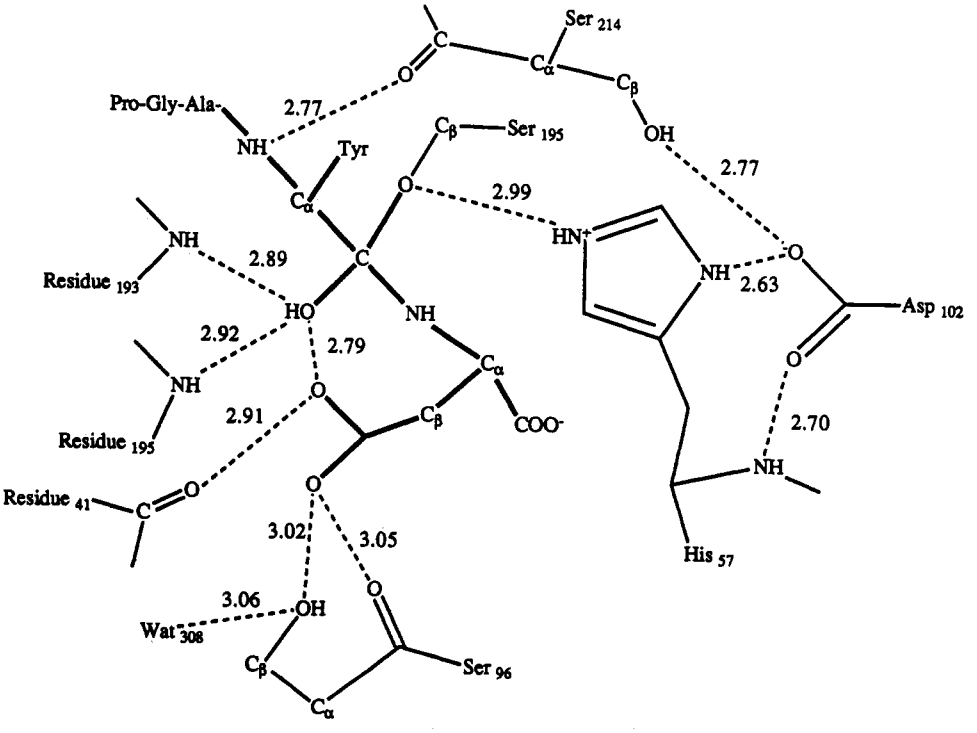

FIGURE 11: Cartoon of the active site. Bold lines indicate the covalent bonds of the tetrapeptide. The observed hydrogen-bonding pattern in the active site is consistent with the neutron structure of trypsin (Kossiakoff & Spencer, 1981) and the solid-state NMR spectrum of α-lytic protease in octane (Burke *et al.*, 1989). The protonation state of the attacking Asp is not clear. The oxygen attached to the tetrahedral carbon has been modeled as an alcohol rather than an alkoxide ion. It is unlikely that an alkoxide ion would be strongly stabilized in hexane.

Despite these questions about the stability of the tetrahedral intermediate in the crystal lattice, it is hard to interpret the electron density shown in Figure 10 (and in the other serine protease structures) as something other than the tetrahedral intermediate. We took great pains not to bias our model toward the tetrahedral intermediate in the active site. Refinement was started with the only high-resolution model of γ-chymotrypsin, with something other than a peptide in the active site (Stoddard *et al.*, 1990). This model has a cinnamate covalently bound to Ser 195. In our initial refinement model, the cinnamate was removed. We would have preferred to start with apo-γ-chymotrypsin, but we (and others) have not been able to completely remove the tetrapeptide from the crystal. Crystallizations that avoid

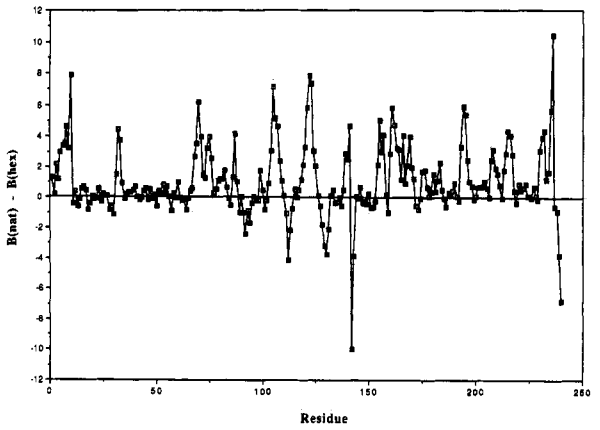

FIGURE 12: Differential temperature factor plot of the backbone atoms of chymotrypsin. The average *B*-value for protein atoms in the hexane structure is 4.4 and in water is 5.4, so that the differences seen in the graph are significant. The graph is predominantly positive, reflecting the rigidity of the enzyme in a hexane environment.

production of the tetrapeptide result in α-chymotrypsin not γ-chymotrypsin. The tetrapeptide was not added to the model until after the solvent structure had been completed. At that point in the refinement, the electron density throughout the map was quite good. Finally, when added, the peptide was modeled as the previously established acyl enzyme adduct with a trigonal carbon. Despite all of these attempts to bias the model away from a tetrahedral geometry, the electron density looks tetrahedral. The native structure that went through an identical protocol of crystallization, data collection, and structural refinement does not exhibit any such departure from the expected acyl enzyme intermediate.

A final point that must be considered is the source of the attacking peptide. The density for the side chain of the attacking peptide is weaker than the density near the tetrahedral carbon, and there is no convincing electron density for the α-carbonyl group. This is probably due to heterogeneity in the attacking peptide. Other studies have shown that there are a large number of peptides in the crystallization buffer (Harel *et al.*, 1991). It is reasonable to assume that some of these peptides were in the solvent channels of the crystal lattice when the crystals were transferred to hexane. These peptides presumably were more soluble in the active site than in hexane.

Moving the crystals into hexane affects the details of the structure of γ-chymotrypsin, but it does not dramatically alter the overall structure. The reactivity of the crystalline enzyme in hexane is similar to that of the enzyme in water in the hydrolysis direction. However, in the absence of water, it is possible to catalyze the reaction in the synthetic direction as well. Chymotrypsin is less mobile in hexane than in water. This decreased mobility, combined with altered side-chain conformations, can be used to explain the altered reactivity of enzymes in organic solvents. The binding of hexane molecules to the surface of chymotrypsin is energetically reasonable, and it may be possible to use organic solvents as a probe of the surface properties of proteins. These binding sites may also be useful in the design of enzyme inhibitors.

ACKNOWLEDGMENT

The authors thank Dr. C. Robert Matthews, Dr. Kenneth M. Merz, Dr. Gregory A. Petsko, Dr. S. Ramaswamy, Dr. Barry L. Stoddard, and Dr. Robert M. Sweet for stimulating discussions. Ms. Beth Buelow grew many of the crystals used in these experiments.

SUPPLEMENTARY MATERIAL AVAILABLE

Tables of hydrogen bond data in hexane and in the native structure and of *R*-factors for the hexane and native structures (12 pages). Ordering information is given on any current masthead page.

REFERENCES

Albery, W. J., & Knowles, J. R. (1986) *Biochemistry 25*, 2572–2577.
Baillargeon, M. W., Laskowski, M., Neves, D. E., Porubcan, M. A., Santini, R. E., & Markley, J. L. (1980) *Biochemistry 19*, 5703–5710.
Bone, R., Shenvi, A. B., Kettner, C. A., & Agard D. A. (1987) *Biochemistry 26*, 7600–7609.
Bone, R., Frank, D., Kettner, C. A., & Agard, D. A. (1989) *Biochemistry 28*, 7600–7614.
Brunger, A. T., Kuriyan, J., & Karplus, M. (1987) *Science 235*, 458–460.
Burke, P. A., Smith, S. O., Bachovchin, W. W., & Klibanov, A. M. (1989) *J. Am. Chem. Soc. 111*, 8290–8291.
Cleland, W. W. (1992) *Biochemistry 31*, 317–319.
Delbaere, L. T. J., & Brayer, G. D. (1985) *J. Mol. Biol. 183*, 89–103.
Dixon, M. M., & Matthews, B. W. (1989) *Biochemistry 28*, 7033–7038.
Dixon, M. M., Brennan, R. G., & Matthews, B. W. (1991) *Int. J. Biol. Macromol. 13*, 89–96.
Fitzpatrick, P. A., Steinmetz, A. C. U., Ringe, D., & Klibanov, A. M. (1993) *Proc. Natl. Acad. Sci. U.S.A. 90*, 8653–8657.
Fletterick, R. J., Sygusch, J., Murray, N., Madsen, N. B., & Johnson, L. N. (1976) *J. Mol. Biol. 103*, 1–13.
Gerlt, J. A., & Gassman, P. G. (1992) *J. Am. Chem. Soc. 114*, 5928–5934.
Gerlt, J. A., & Gassman, P. G. (1993) *J. Am. Chem. Soc. 115*, 11552–11568.
Gerlt, J. A., Kozarich, J. W., Kenyon, G. L., & Gassman, P. G. (1991) *J. Am. Chem. Soc. 113*, 9667–9669.
Gololobov, M. Y., Voyushina, T. L., Stepanov, V. M., & Adlercreutz, P. (1992) *FEBS Lett. 307*, 309–312.
Harel, M., Su, C.-T., Frolow, F., Silman, I., & Sussman J. L. (1991) *Biochemistry 30*, 5217–5225.
Hartley, B. S., & Kilby, B. A. (1954) *Biochem. J. 56*, 288–297.
Hartsough, D. S., & Merz, K. M., Jr. (1992) *J. Am. Chem. Soc. 114*, 10113–10116.
Hartsough, D. S., & Merz, K. M., Jr. (1993) *J. Am. Chem. Soc. 115*, 6529–6537.
Henderson, R. J. (1970) *J. Mol. Biol. 54*, 341–354.
Hodel, A., Kim, S. H., & Brunger, A. T. (1992) *Acta Crystallogr. A48*, 851–858.
Homandberg, G. A., Mattis, J. A., & Laskowski, M., Jr. (1978) *Biochemistry 17*, 5220–5227.
James, M. N. B., Sielecki, A. R., Brayer, G. D., Delbaere, L. T. J., & Bauer, C. A. (1980) *J. Mol. Biol. 144*, 43–88.
Jones, T. A., Zou, J. Y., Cowan, S. W., & Kjeldgaard, M. (1991) *Acta. Crystallogr. A47*, 110–119.
Kasche, V., Michaelis, G., & Galunsky, B. (1991) *Biotechnol. Lett. 13*, 75–80.
Kossiakoff, A. A., & Spencer, S. A. (1981) *Biochemistry 20*, 6462–6474.
Kuhl, P., Halling, P. J., & Jakubke, H. D. (1990) *Tetrahedron Lett. 31*, 5213–5216.
Marquart, M., Walter, J., Deisenhofer, J., Bode, W., & Huber R. (1983) *Acta Crystallogr. B39*, 480–490.
Matthews, D. A., Alden, R. A., Birktoff, J. J., Freer, S. T., & Kraut J. (1975) *J. Biol. Chem. 250*, 7120–7126.
Monahan, J. E., Schiffer, M., & Schiffer, J. P. (1967) *Acta Crystallogr. 22*, 322.
Ooi, T., & Oobataka, M. (1988) *J. Biochem. 103*, 114–120.
Perona, J. J., Craik, C. S., & Fletterick, R. J. (1993) *Science 261*, 620–621.

Petsko, G. A. (1985) *Methods. Enzymol. 114*, 141–146.
Polgar, L. (1987) in *Hydrolytic Enzymes* (Neuberger, A., & Brocklehurst, K., Eds.) Chapter 3, pp 159–200, Elsevier Science Publishers B. V. (Biomedical Division), Amsterdam.
Pompliano, D. L., Peyman, A., & Knowles, J. R. (1990) *Biochemistry 29*, 3186–3194.
Richarz, R., Tschesche, H., & Wüthrich, K. (1980) *Biochemistry 19*, 5711–5715.
Rühlmann, A., Kukla, D., Schwager, P., Bartels, K., & Huber R. (1973) *J. Mol. Biol. 77*, 417–436.
Sharp, K. A., & Honig, B. (1990) *Annu. Rev. Biophys. Biophys. Chem. 19*, 301–332.
Singer, P. T., Smålas, A., Carty, R. P., Mangel, W. F., & Sweet, R. M. (1993a) *Science 259*, 669–673.
Singer, P. T., Smålas, A., Carty, R. P., Mangel, W. F., & Sweet, R. M. (1993b) *Science 261*, 621–622.
Stahl, M., Mansson, M. O., & Mosbach, K. (1990) *Biotechnol. Lett. 12*, 161–166.
Steitz, T. A., & Shulman, R. G. (1982) *Annu. Rev. Biophys. Bioeng. 11*, 419–444.
Stoddard, B. L., Bruhnke, J., Proter, N., Ringe, D., & Petsko, G. A. (1990) *Biochemistry 29*, 4871–4879.
Sweet, R. M., Wright, H. T., Janin, J., Chothia, C. H., & Blow, D. M. (1974) *Biochemistry 13*, 4212–4228.
Tawaki, S., & Klibanov, A. M. (1992) *J. Am. Chem. Soc. 114*, 1882–1884.
Tskuada, H., & Blow, D. M. (1985) *J. Mol. Biol. 184*, 703–711.
Tulinsky, A., & Blevins, R. A. (1987) *J. Biol. Chem. 262*, 7737–7743.
West, J. B., Hennen, W. J., Lalonde, J. L., Bibbs, J. A., Zhong, Z., Meyer, E. F., Jr., & Wong, C. H. (1990) *J. Am. Chem. Soc. 112*, 5313–5320.
Wilks, H. M., Hart, K. W., Feeney, R., Dunn, C. R., Muirhead, H., Chia, W. N., Barstow, D. A., Atkinson, T., Clarke, A. R., & Holbrook, J. J. (1988) *Science 242*, 1541–1544.
Zaks, A., & Klibanov, A. M. (1984) *Science 224*, 1249–1251.
Zaks, A., & Klibanov, A. M. (1985) *Proc. Natl. Acad. Sci. U.S.A. 82*, 3192–3196.
Zaks, A., & Klibanov, A. M. (1986) *J. Am. Chem. Soc. 108*, 2767–2768.
Zaks, A., & Klibanov, A. M. (1988a) *J. Biol. Chem. 263*, 3194–3201.
Zaks, A., & Klibanov, A. M. (1988b) *J. Biol. Chem. 263*, 8017–8021.